# AT622 Section 14
# Particle Scattering

The aim here is to provide a conceptual grasp of particle scattering without inundating with complicated recipes.

Particle scattering is a complex topic—but we can simplify the view of particle scattering by visualizing the scattered radiation as composed of contributions of many waves generated by oscillating dipoles that make up the particle (Fig. 14.1). The complication is that each dipole affects the other such that the resulting field emitted by an oscillating dipole has a contribution that is due to stimulation by the incident field and a contribution due to stimulation by the fields of neighboring dipoles. Another complication is that the charge distribution in the particle forms higher order poles than dipoles and these multipoles also contribute to the scattered radiation.

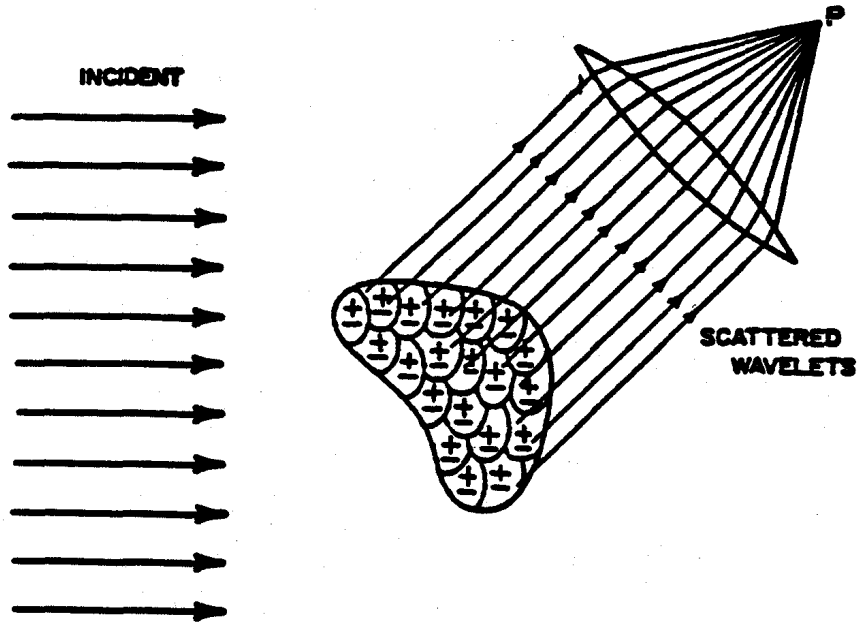


*Fig. 14.1 The radiation scattered by a particle and observed at P results from the superposition of all wavelets scattered by the subparticle regions (dipoles)—from Bohren and Huffman (1983).*

## 14.1 Scattering by a Single Dipole: Rayleigh Scattering

Assume that a spherical wave is emitted from a (spherical) dipole, i.e.,

$$\mathcal{E} \rightarrow \frac{\mathcal{E}_o}{kr} e^{-i\Phi}$$

where $\Phi = (kr - \omega t)$ is the phase of wave and $k$ is the wavenumber. Based on arguments of geometry

$$\mathcal{E}_r = \mathcal{E}_{or}\left[\frac{e^{-ik(r-ct)}}{r}\right]k^2\alpha$$
$$\mathcal{E}_t = \mathcal{E}_{o\ell}\left[\frac{e^{-ik(r-ct)}}{r}\right]k^2\alpha\cos\theta \qquad (14.1)$$

where $\alpha$ is the polarizability (this is a parameter that is a 'measure' of how readily matter polarizes charges—refer to Section 4), and where radiation scattered by a single oscillating dipole is a spherical wave, which is represented by the factor in parentheses. In terms of intensities, the two components of polarized radiation therefore take the form

$$I_r = I_{or}k^4\,|\alpha|^2\,/\,r^2$$
$$I_\ell = I_{o\ell}k^4\,|\alpha|^2\cos^2\theta \qquad (14.2)$$

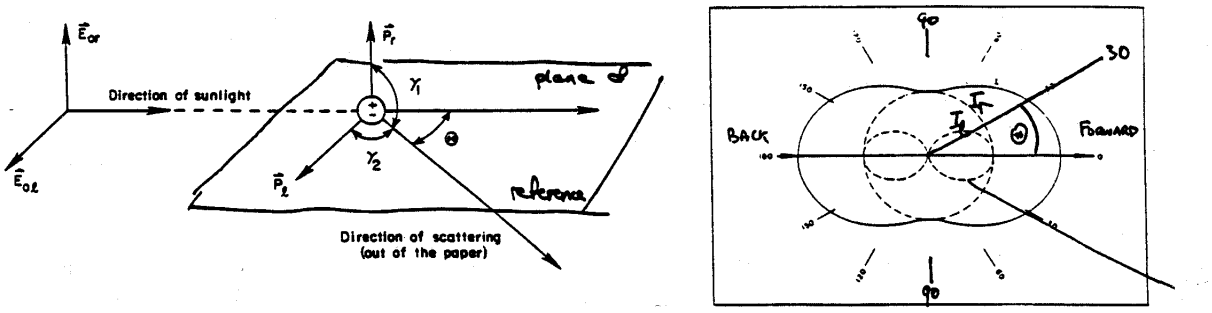


*Fig. 14.2 (a) Geometry for scattering by a single dipole. Shown are the plane of reference and the orthogonal components of both the electric field and the dipole moment, which lie parallel and perpendicular to the plane. The scattering angle $\theta$ is defined on this plane. (b) Scattering pattern of a single dipole.*

A special but nonetheless important case applies to an unpolarized beam of radiation, like sunlight, scattered by small particles. Unpolarized radiation can be viewed as a mixture of two independent linearly polarized beams of the same intensity. Therefore $I_{or} = I_{o\ell} = I_o/2$ and

$$I = \frac{1}{2}(I_\ell + I_r) = \frac{I_o}{2}[1+\cos^2\theta]k^4\,|\alpha|^2\,/\,r^2 \qquad (14.3)$$

describes the scattered intensity of unpolarized radiation by small particles. The scattering pattern predicted by Eqn. (14.3) is also shown in Fig. 14.3 for unpolarized incident radiation.

There are a number of consequences of Eqn. (14.3) including:

- under pure Rayleigh scattering as much radiation is scattered forward as backwards
- at $\theta = 90$, Rayleigh scattering completely polarizes unpolarized incident light (such as from the sun).
- the amount (i.e., intensity) of light scattered varies as $k^4$ or as $\lambda^{-4}$. Consequently, the blue portions of white light are preferentially scattered whereas the red portions of white light are preferentially transmitted.

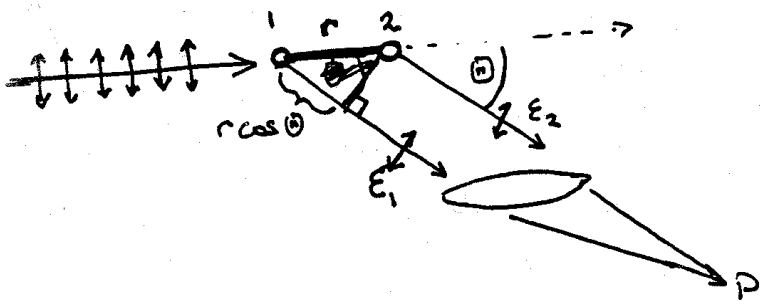


*Fig. 14.3 Two isolated dipoles emit waves in all directions. At some point P far from the 'particle', these waves superimpose to create the scattered wave along the direction θ. These waves either constructively or destructively interfere depending on their relative phase difference ΔΦ, which is defined in terms of the extra distance the incident wave travels first to the second dipole (r) less the extra distance from the first dipole to P(r cos θ).*

## 14.2 Radiation From Multiple Dipoles: Towards Understanding Scattering by Large Particles

Phase difference between waves 1 and 2 (simply proportional to the difference in path length)

$$\Delta\Phi = \frac{2\pi r}{\lambda}(1 - \cos\theta)$$

The EM waves from dipoles 1 and 2 superimpose (i.e., they add)

$$\mathcal{E}_{1+2} = \mathcal{E}_1 e^{i\Phi} + \mathcal{E}_2 e^{i\Phi+\Delta\Phi} \tag{14.4}$$

and in terms of intensity (= radiance, which is proportional to $|\mathcal{E}|^2$)

$$I(=N)_{1+2} = \text{constant}[\mathcal{E}_1^2 + \mathcal{E}_2^2 + 2\mathcal{E}_1\mathcal{E}_2\cos\Delta\Phi] \tag{14.5}$$

(Assume $\mathcal{E}_1 = \mathcal{E}_2$). Now for certain phase conditions, such as $\Delta\Phi = \pi, 3\pi, \ldots$ the fields cancel (are out of phase). For other conditions, $\Delta\Phi = 0, 2\pi, \ldots$ and the fields reinforce (Fig. 14.4a). The latter condition is always met in the forward direction, -*M* radiating dipoles (Fig. 14.4b) each radiating with an intensity *I* at $\theta = 0$ produces an intensity which *is* $M^2$ times the intensity of a single dipole in the forward direction. Some other general inferences are

- The larger the particle, more radiation is scattered forward
- The larger the ratio $2\pi r/\lambda$ (size parameter) the more convoluted is the scattering (i.e., more maxima and minima are expected as $\theta$ is varied, e.g., Fig. 14.5).

Although the simple discussion of multiple dipoles given above ignores the complicating effects of dipole-dipole interactions, the broad behavior predicted carries over to the more complete calculation of particle scattering illustrated, for example, in Fig. 14.5.

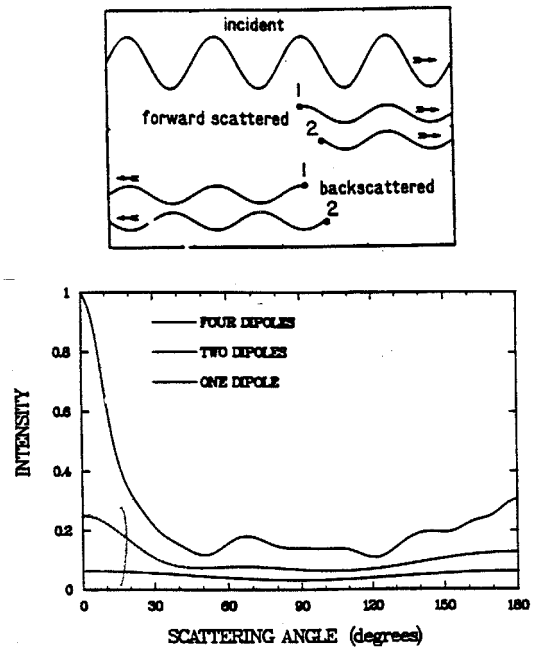


*Fig. 14.4 (a) Excited by an incident wave, two dipoles scattering all directions. In the forward direction, the two waves are exactly in phase regardless of the separation of dipoles. (b) The greater the number of dipoles in the particle array, the more they collectively scatter toward the forward direction, For the example shown here, all dipoles lie on the same line, are separated by one wavelength, and interact with each other. The scattered intensity is obtained as an average over all orientations of the line of dipoles (from Bohreu, 1988).*

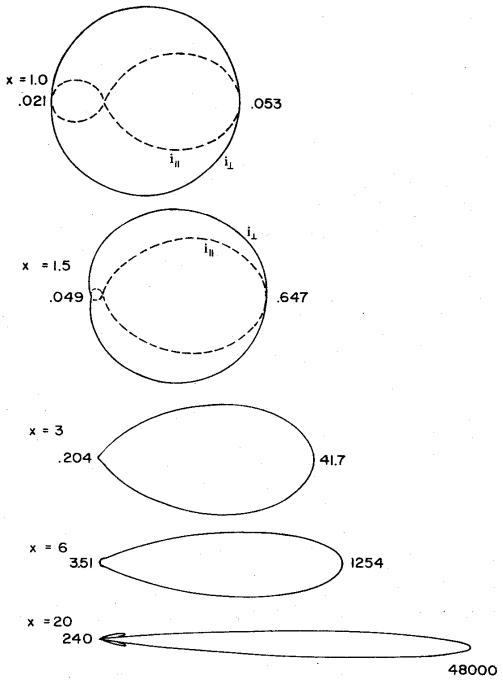


*Fig. 14.5 Polar plots of the scattered intensity for the values of size parameter stated derived from Lorentz-Mie theory. The numbers indicate magnitudes in the forward and backward directions (note the scale change) - from Bohren and Huffman (1983).*

## 14.3 Particle Extinction

Forward scattering is a special measure of the totality of the interaction. Depletion of forward propagating radiation is referred to as extinction, BUT we cannot distinguish scattering from absorption along this direction. So in addition to a measure of extinction (this is measured by the extinction coefficient), we also need a parameter that defines the ratio of extinction by scattering to extinction by absorption. This ratio defines the single scatter albedo

$$\tilde{\omega}_o = \frac{\text{amount of scattering}}{\text{total extinction}} = \text{single scattering albedo}$$

$$\tilde{\omega}_o = 1 \text{ all scattering (conservative)}$$

$$\tilde{\omega}_o = 0 \text{ all absorption (absorptive).}$$

Some idea of the general properties of $\tilde{\omega}_o$ for spherical particles of a size that is typically found in clouds is provided in Figs. 14.6a and b. Example spectra of $\tilde{\omega}_o$ for 5 and 50 μm water and ice spheres are shown for wavelengths between 0.3 and 50 μm. The spectra presented in these diagrams illustrate a number of important properties of $\tilde{\omega}_o$:

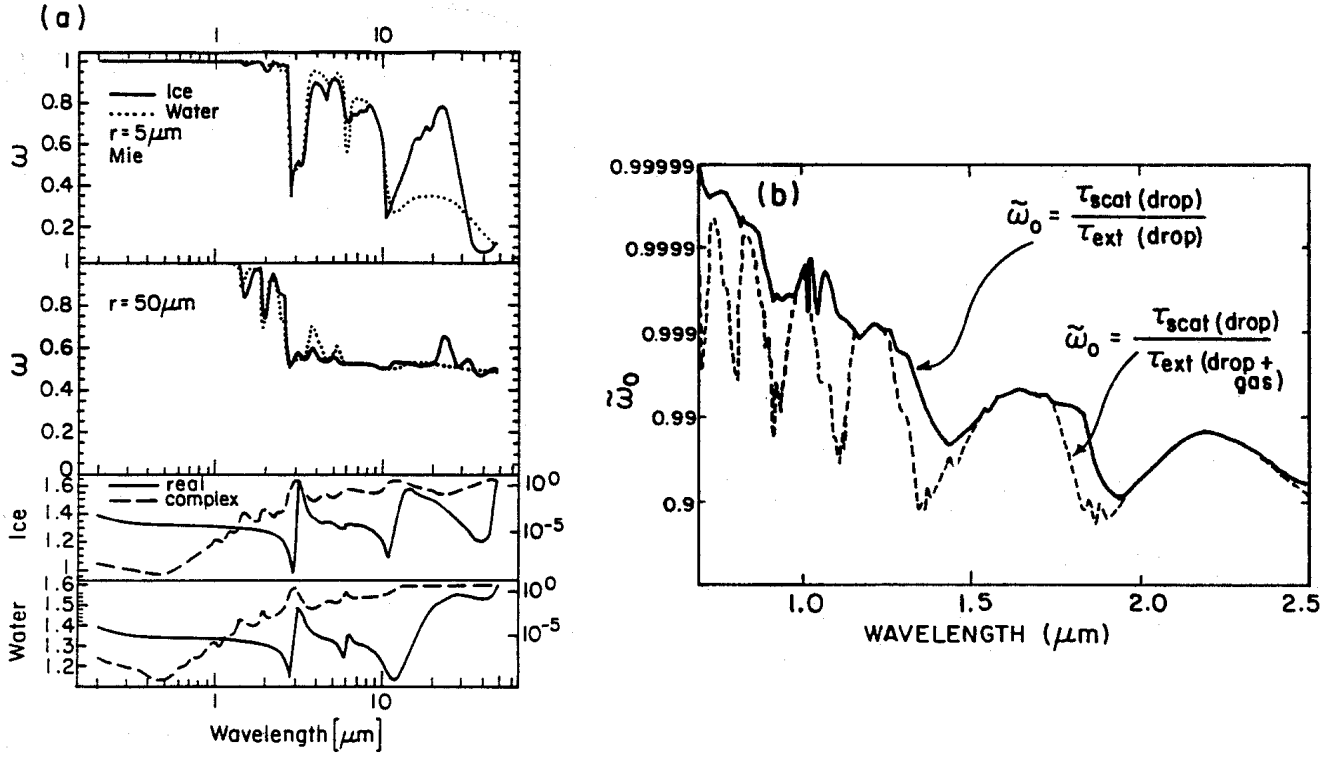


*Fig. 14.6 (a) The single scatter albedo as a function of λ for 5 μm water and ice spheres. (b) The single scatter albedo of a model cloud as a function of wavelength. The solid line refers to droplet absorption alone, whereas the dashed line to droplet plus vapor absorption (from Twomey and Seton, 1980).*

- values of $\tilde{\omega}_o \geq 0.99$ are typical of wavelengths less than about 1.5 μm (this is made clear in Fig. 14.6b). The spectra of $\tilde{\omega}_o$ in the visible and near infrared region is actually complex.

- The minima in $\tilde{\omega}_o$ represent absorption features by ice and water and these align with the corresponding maxima of the complex part of the refractive index $\kappa$. This is consistent with our expectations from the simple theories described below.

    - Particle absorption (to the extent it is defined by the co-albedo 1-$\tilde{\omega}_o$) is dependent on particle radius.
    - There are a number of spectral regions where the differences in $\tilde{\omega}_o$ between ice and water spheres are large. Differences that exist in the near infrared region (such as near 1.6 μm) cannot be seen but others can.

    - The single scatter $\tilde{\omega}_o$ is a volumetric quantity defined as the ratio of the scattering properties of the volume to the properties that define the total extinction by the volume. For most wavelengths of interest, this extinction is a result of both absorption and scattering by cloud particles as well as absorption by the minor gases in the volume, especially water vapor. An example of the effects of water vapor absorption on $\tilde{\omega}_o$ over the wavelength range 0.5 to 2.5 μm is presented in Fig 14.6b. What makes the problem of multiple scattering particularly troublesome at these wavelengths is the fact that both liquid water and bands containing thousands of water vapor lines overlap in the same spectral region.

*(a) Cross Sections and Efficiencies*

Particle extinction is conveniently defined in terms of a quantity called the extinction efficiency $Q_{ext}$ way of visualizing this quantity (but not an entirely correct way) is provided by reference to Fig 14.7. In this simplistic view, we consider radiation as a stream of photons that flow into a volume containing the scattering particles. Each particle within the volume blocks a certain amount of radiation resulting in a reduction of the amount of radiation directly transmitted through the volume. The reduction in the radiation as it passes through a volume of spheres can be expressed in terms of a cross-sectional area $C_{ext}$, which is generally different from the geometric cross-sectional area of the particle. For spherical particles of radius $r$, the definition of $Q_{ext}$ then follows as

$$Q_{ext} = \frac{C_{ext}}{\pi r^2}. \tag{14.6}$$

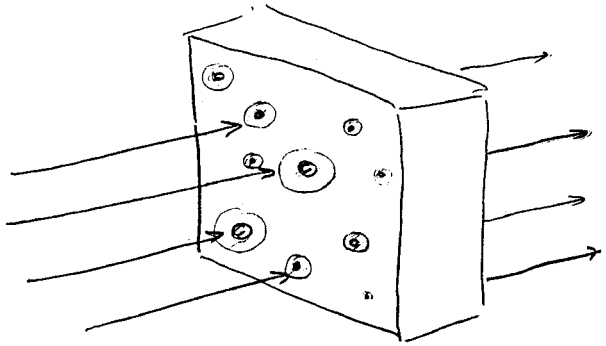

*Fig. 14.7 An approximate view of particle extinction. Particles 'block' a certain amount of radiation from penetrating through the slab. The reduced transmission can be described in terms of a cross-sectional area $C_{ext}$ shown as the shaded area around the particle. While this view of extinction is a simple one, to visualize it is not entirely correct as extinction occurs through subtle interference effects.*

When $C_{ext}$ exceeds the value of the geometrical cross-sectional area of the particle, $Q_{ext} > 1$ and more radiation is attenuated by the particle than is actually intercepted by its physical cross-sectional area. Since this extinction occurs by absorption or by scattering or by a combination of both, it follows that

$$Q_{ext} = Q_{abs} + Q_{sca} . \tag{14.7}$$

We expect that $Q_{ext}$ depends on the refractive index of the material, the wavelength of radiation and the size of the particle. Figure 14.8 shows a plot of $Q_{ext}$, calculated from Lorentz-Mie theory, as a function of the size parameter $x$ for water sphere illuminated by light of a wavelength of 0.5 μm. Somewhat obvious are the large maxima and minima with a superposition of finer scale variations (referred to as ripples). Another familiar phenomenon that follows from consideration of Fig. 14.8 *is* the *reddening* of white light as it passes through a collection of small particles. This is depicted by the rapid rise in extinction as $x$ increases (i.e., toward shorter wavelengths) and is a general characteristic of nonabsorbing particles that are smaller than the incident wavelength. Thus, blue light is extinguished (scattered) more than red light, leaving the transmitted light reddened in comparison to the incident light. This reddening is a phenomenon that is not only limited to sunlight in the Earth's atmosphere but also for starlight reddened by interstellar dust particles. It is obvious from Fig. 14.8 that extinction is highly dependent on the size of the particle.

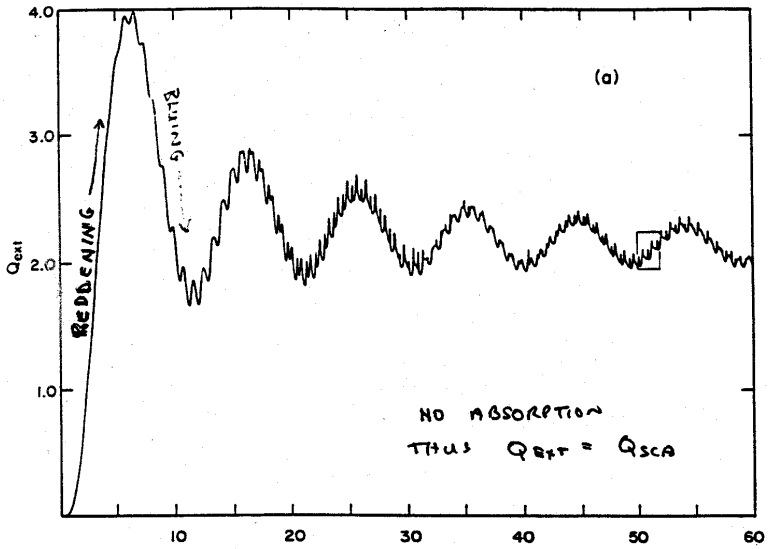


*Fig. 14.8 Extinction efficiency for water droplet in air calculated for $\lambda = 0.51$ μm as a function of size parameter x. There are two ways of presenting results of this type. For the example shown, the size parameter can also be varied by changing the wavelength, while fixing the size of the particle. The results are not the same because as wavelength varies so does the refractive index and extinction depends not only on the size parameter but also on the refractive index (adapted from Bohren and Huffman, 1983).*

*(b) Extinction by a Cloud of Many Particles*

The opposite spectral effect of reddening is the blueing of transmitted white light that occurs as the extinction decreases with increasing $x$ on the high $x$ side of the extinction peaks shown in Fig. 14.8. Unlike reddening, this blueing phenomenon is highly dependent on the character of the particle size distribution and occurs rarely: "once in a blue moon." In fact, this extinction feature and others that depend on particle size are obscured, if not totally obliterated, when the extinction is determined from observations of light scattered by a small volume of air containing particles of a variety of sizes. Under

atmospheric conditions, the intensity of radiation scattered by such a volume of particles may be simply obtained as the addition of the intensities of light scattered by individual particles.

Suppose

$$n(r) = \text{constant}\, r^{(1-3b)/b} e^{-r/r_m}, \tag{14.8}$$

represents the size distribution of (say) water droplets in a given volume of cloud. Some basic properties of this distribution are:

- $r_{mode} = (b - 1)r_m$
- $r_{mean} = br_m$
- $r_e = \dfrac{V}{A} = \dfrac{\int n(r) r^3 dr}{\int n(r) r^2 dr} = (b + 2)r_m$
- $LWC = \dfrac{4}{3}\pi\rho_{water} N_o r_m^3 f(3); \qquad f(\ell) = \dfrac{\Gamma(b + \ell)}{\Gamma(b)}$
- $A = \pi \int n(r) r^2 dr = \pi N_o r_m^2 f(2)$

The parameter *b is* a measure of the distribution variance and thus the width of the distribution. When the scattered fields from all particles in the volume are added, we see a general smoothing of the extinction spectrum as *b* increases. The very fine ripple structure in extinction for the monodispersed cloud (i.e., $b = 0$) disappears as *b* is systematically increased from zero and the interference structure (i.e., the broad maxima and minima) eventually fades away as the distribution widens. For the widest distributions chosen for this illustration ($b = 0.5$), the only remaining features are reddening at small size parameters, and, the asymptotic approach to the limiting value 2.

*(c) The Extinction Paradox*

Another important feature of the $Q_{ext} - x$ spectrum is the tendency for the extinction $Q_{ext}$ either to oscillate around the value of 2 as $x \rightarrow \infty$ as illustrated in Fig. 14.8 or to converge to the value of 2 as in the cases of Fig. 14.9. This behavior of particle extinction is referred to as the *extinction paradox.* Why a paradox? Intuition suggests that if we consider extinction as just the radiation that is blocked by the particle, like that illustrated in Fig. 4.7, then the extinction cross section is just the shadow projected by the very large particle. This geometrical view of extinction predicts that the limiting value of $Q_{ext}$ is 1 and not 2. However, no matter how large the particle, it still has an edge, and in the vicinity of the edge rays do not behave the way our simple geometrical arguments say they should. The energy removed from the forward direction can be thought of as being made up of a part that represents the amount blocked by the cross-sectional area of the particle and a part diffracted around the particle's edge. The diffracted amount eventually fills in the shadow area when viewed far enough from the particle. The total amount removed from the incident beam by diffraction is therefore also characterized by the particle cross-sectional area. The net result is that an amount twice the cross-sectional area of the particle is scattered out of the incident beam. We learn from this, and further discussion below, that particle extinction is not just a process of blocking light, but is actually a result of more subtle interference effects (Fig. 14.10).

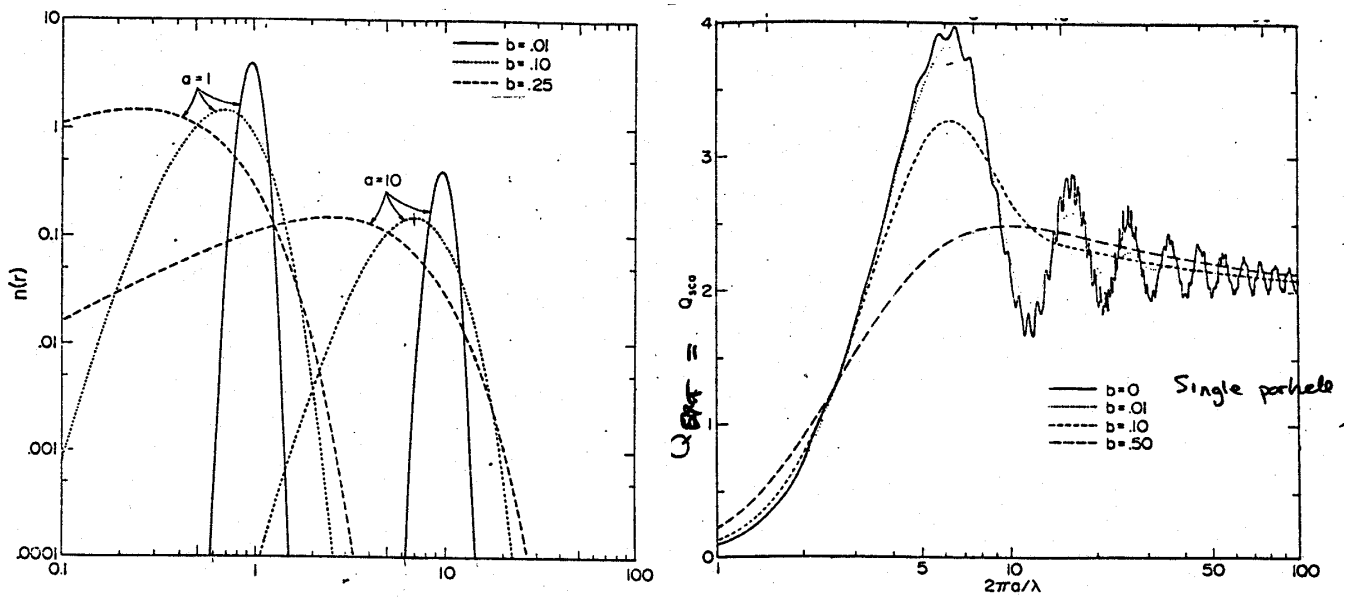


*Fig. 14.9 (a) Standard size distribution (14.8) for 2 values of a and three values of b. The size distribution is normalized so that the integral over all sizes is N = 1. (b) The extinction efficiency, $Q_{ext}$, as a function of the effective size parameter $x = 2\pi a/\lambda$ for the values of effective variance b given. Mie theory was used with a refractive index $n' = 1.33$, $\kappa = 0$ (after Hansen and Travis 1974).*

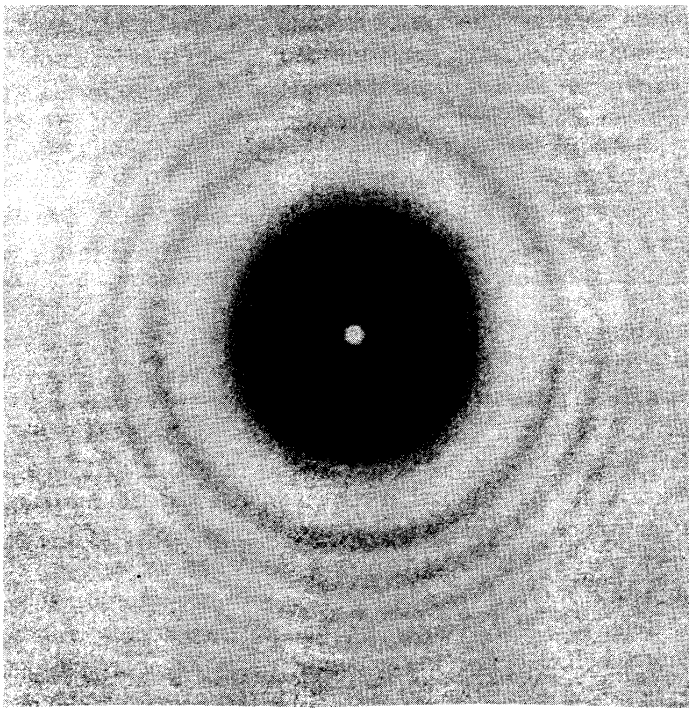

*Fig. 14.10 An illustration of the extinction paradox. The photograph shows the diffraction pattern produced by a round stop. In the middle is the Poisson spot. The image is created by observing a light source obscured at some distance by a ball bearing of 10 mm diameter. The telescope is located several meters behind this obstacle.*

## 14.4 A Simple Model of Particle Extinction

General references:

Van deHulst, 1957: Chapts. 3 and 11

Stephens, 1984: *Appl. Opt*., **23**, 954-959.

Ackerman S. and G.L. Stephens, 1987 *J. Atmos. Sci.,*

G.L. Stephens, 1994: *Remote Sensing.,*

*(a) Fundamental Extinction Formula*

Consider a plane wave incident on a particle that we choose to write as

$$\mathcal{E}_o = e^{-ikz+iwt} \tag{14.9}$$

where we conveniently assume the wave has a unitary amplitude.

Suppose the scattered wave at $O'$ in Fig. 14.11 is a spherical wave of the form[1]

$$\mathcal{E}_{sca} = S(\theta)\frac{e^{-ikr+iwt}}{ikr} \tag{14.10}$$

that introduces the function $S(\theta)$, which we hereafter refer to as the amplitude function. This function accounts for the fact that the intensity of the scattered radiation varies with scattering angle $\theta$. Now extinction is defined at $\theta = 0$ and $C_{ext}$ can be derived in terms of $S(\theta)$—this relation is known as the fundamental extinction formula. In deriving this relation, consider points near $\theta = 0$ such that[2]

$$r \approx z + \frac{x^2 + y^2}{2z}$$

provided $x, y << z$. The resultant wave is

$$\begin{aligned}\mathcal{E}_{sca} + \mathcal{E}_o &= \frac{S(\theta=0)}{ikz}e^{-ik(z+(x^2+y^2)/2z)+iwt} + e^{-ikz+iwt} \\ &= \mathcal{E}_o\left[1 + \frac{S(\theta=0)}{ikz}e^{-ik(x^2+y^2)/2z}\right]\end{aligned}$$

[1] In the derivation of Van deHulst (1957, p.29), the complex factor $i$ appears in the denominator for reasons that become evident in his derivation of cross sections. We will not outline these derivations here and choose to omit this factor in our discussion.

[2] $$\left[r = (z^2 + x^2 + y^2)^{1/2} = z\left(1 + \frac{x^2 + y^2}{z^2}\right)^{1/2} \approx z\left(1 + \frac{x^2 + y^2}{2z^2}\right)\right]$$

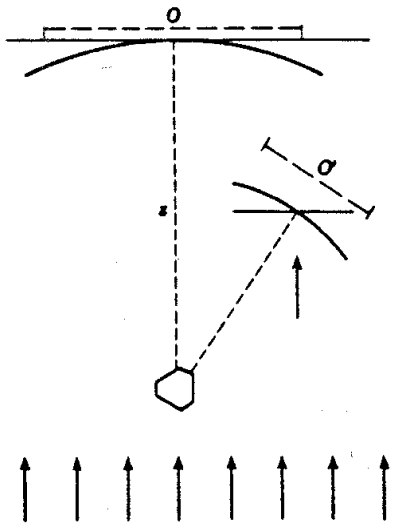


*Fig. 14.11 An arbitrary particle that scatters a plane wave to the point O'.*

The intensity is obtained by squaring the modulus of this expression

$$I(x,y) \approx |\, E + E_o \,|^2 = |\, E_o \,|^2 \left[ 1 + \frac{2}{kz} \Re e \left\{ \frac{S(\theta = 0)}{i} e^{-ik(x^2+y^2)/2z} \right\} \right]$$

Now, the total intensity is

$$\int_{area} \int I(x,y)dxdy \Rightarrow I_o \iint dxdy + \frac{2I_o}{kz} \iint \Re \left[ \frac{S(\theta = 0)}{i} e^{-ik(x^2+y^2)/2z} \right] dxdy \qquad (14.11)$$
$$\approx O - C$$

where $O$ is the integral of the first term and corresponds to the geometric area projected by the particle on a distant screen and $C$ is the integral of the second term and can be interpreted as the amount of light reduced by the presence of the particle (due to extinction). This integral reduces to

$$C_{ext} = \frac{4\pi}{k^2} \Re e[S(\theta = 0)]; \quad \text{thus, } Q_{ext} = \frac{4}{x^2} \Re e[S(\theta = 0)]. \qquad (14.12)$$

*(b) Anomalous Diffraction Theory*

One may gain the false impression, both from Fig. 14.7 and from the arguments leading to Eqn. (14.12) that extinction occurs through blocking an amount of incident light of magnitude $C_{ext}$. In fact, extinction is a subtle interference phenomenon and not one of merely a blocking of light as the extinction paradox reminds us. In discussing this paradox, we learn that the particle not only 'blocks' an amount of light that is defined by the geometric cross section but also removes some of the energy of the original wave via interference. A relatively simple, but nonetheless useful model of extinction is provided by the anomalous diffraction theory of Van de Hulst (1957, Ch. 11), which seeks to model these interferences.

In the ADT of van de Hulst, we are interested in defining the characteristics of the wave on a reference "screen" $V$ far removed from the particle (Fig. 14.12). We argue that the characteristics of this

wave at $V$ are governed only by diffraction resulting from interference between the ray just outside the particle to one that passes through the particle. A difference in phase between these rays creates this interference. The basis that we claim these can interfere results from considering that $V$ is infinitely far from the particle and that the particle is both large (such that we can trace rays through it and 'soft' so that refraction at the surface interface is negligible).

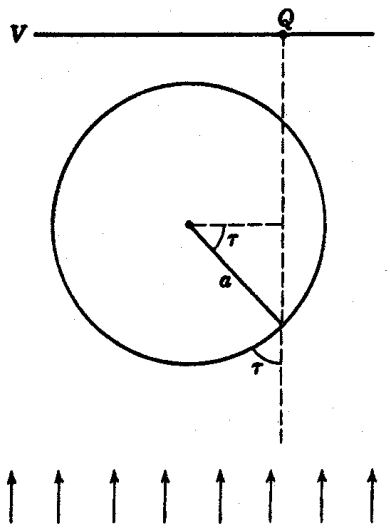


*Fig. 14.12 Ray passing through sphere.*

We begin by noting that the extinction paradox predicts

$$C_{ext} = 2G \tag{14.13}$$

where $G$ is the geometric cross section leading to a value of $Q_{ext} = 2$ when $r \to \infty$. From this and Eqn. (14.12) it follows that

$$S(\theta = 0) = \frac{k^2}{2\pi} G \tag{14.14}$$

Now consider a transparent particle with a ray traversing it along the direction drawn in Fig. 14.12. The phase difference between the ray outside the particle to the ray that penetrates the particle at an angle $\varphi$ as shown in Fig. 14.12 is

$$\Delta\phi = 2x(m-1)\sin\varphi = \rho\sin\varphi$$

where $\rho$ defines the phase shift of the central ray. At point $Q$ the amplitude $\mathcal{E}_Q$ is

$$\mathcal{E}_Q = e^{-\Delta\phi} = e^{-i\rho\sin\varphi}$$

for an amplitude of the incident wave $\mathcal{E}_o$. Thus the net attenuation is

$$S(\theta = 0) = \frac{k^2}{2\pi} \iint [1 - e^{-i\rho \sin \varphi}] dx dy$$

where the integral is taken over the geometric shadow area of the particle. With substitution and change of coordinates, the above integral can be evaluated (refer Van de Hulst, p175) to yield

$$S(\theta = 0^\circ) = x^2 K(i\rho) \tag{14.15}$$

where

$$K(w) = \frac{1}{2} + \frac{e^{-w}}{w} + \frac{e^{-w} - 1}{w^2},$$

and thus

$$Q_{ext} = 4\Re e(K(i\rho)). \tag{14.16}$$

Figure 14.13 shows examples of $Q_{ext}$ calculated using this simple formula and compares it to the Lorentz-Mie formula. Clearly the approximate formula has some shortcomings (no ripple structure) but the overall characteristics of the $Q_{ext}$ curves are well represented (especially as $m \rightarrow 1$). The simple theory also allows us to interpret the larger maxima and minima as interference features. The approach is very simple and readily adapted to non-spherical particles. It may prove to be a desirable way of incorporating scattering parameters into atmospheric circulation models for example.

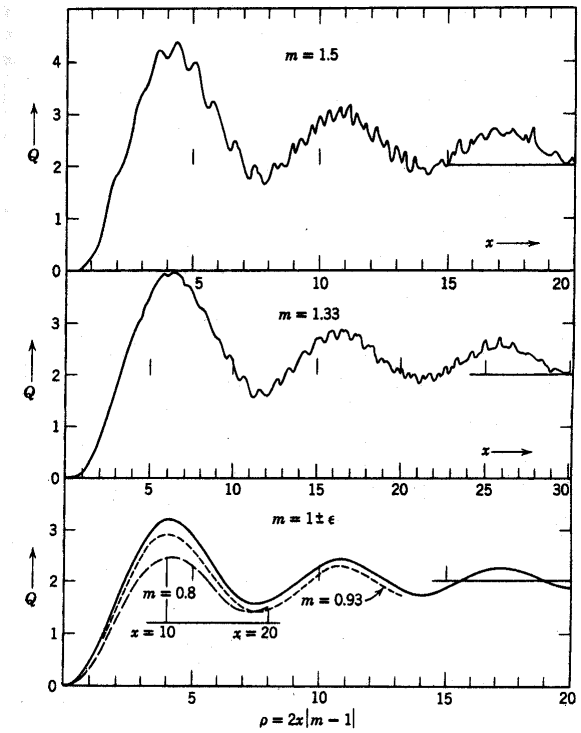


*Fig. 14.13 Extinction curves computed from Mie's formulas for m = 1.5, 1.33, 0.93, and 0.8. The scales of x have been chosen in such a manner that the scale of $\rho = 2x \mid m - 1 \mid$ is common to these four curves and to the extinction curve for $m - 1 = \pm\varepsilon$ .*

Absorbing particles can also be simply handled in the ADT approach. If $m = n - i\kappa$, then we can define the quantity

$$\tan\beta = \frac{\kappa}{n-1}$$

and note that $\beta$ is very small for most solar wavelengths (see Fig. 14.14).

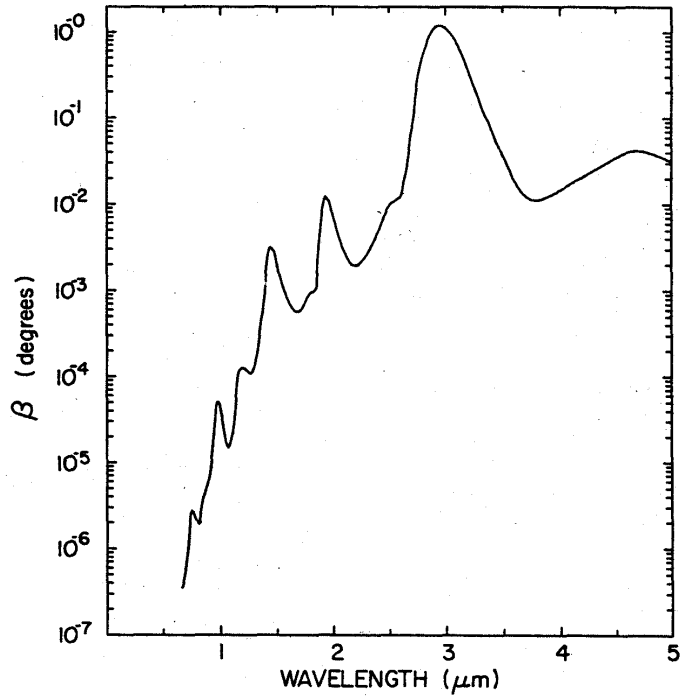


*Fig. 14.14 The angle as a function of wavelength for water*

The phase shift of the central ray is then

$$\rho^* = 2x(m-1) = \rho(1 - i\tan\beta) \tag{14.17}$$

where $\rho = 2x(n - 1)$ and from Eqn. (14.16)

$$Q_{ext} = 4\Re e[K(i\rho + \rho\tan\beta)] \tag{14.18}$$

The energy absorbed inside the sphere is simply calculated by considering the dampening factor of the wave in the particle. The waveform is

$$\exp(-i\rho^*\sin\tau) \rightarrow \exp[-2x\kappa\sin\tau] \quad \exp[-i\rho\sin\tau].$$

The decrease in **intensity** on passage through the particle is therefore

$$1 - e^{-4x\kappa\sin\varphi}$$

which is due to absorption. Thus

$$Q_{abs} \cong \frac{1}{\pi r^2} \iint [1 - e^{-4x\kappa \sin\varphi}] dxdy$$

and

$$Q_{abs}\, 2K(4x\kappa) \tag{14.20}$$

where $v = 4x\kappa$ serves as a particle absorption similarity parameter—i.e., absorption by two particles one of radius $a_1$ and composition $\kappa_1$, and the other of radius $a_2$ and composition $\kappa_2$, are identical (self similar) when $v_1 = v_2$ . Figure 14.15 presents a plot of $Q_{abs}$ as a function of $v$ from Eqn. (14.20) and contrasts this with efficiencies derived from Lorentz-Mie theory, assuming ice spheres. The ADT results match those of Lorentz-Mie when $v$ is small (which is the range of validity of the ADT). Spectra of $Q_{abs}$, also indicate reasonable agreement and serve to remind us that this absorption is sensitive to particle size.

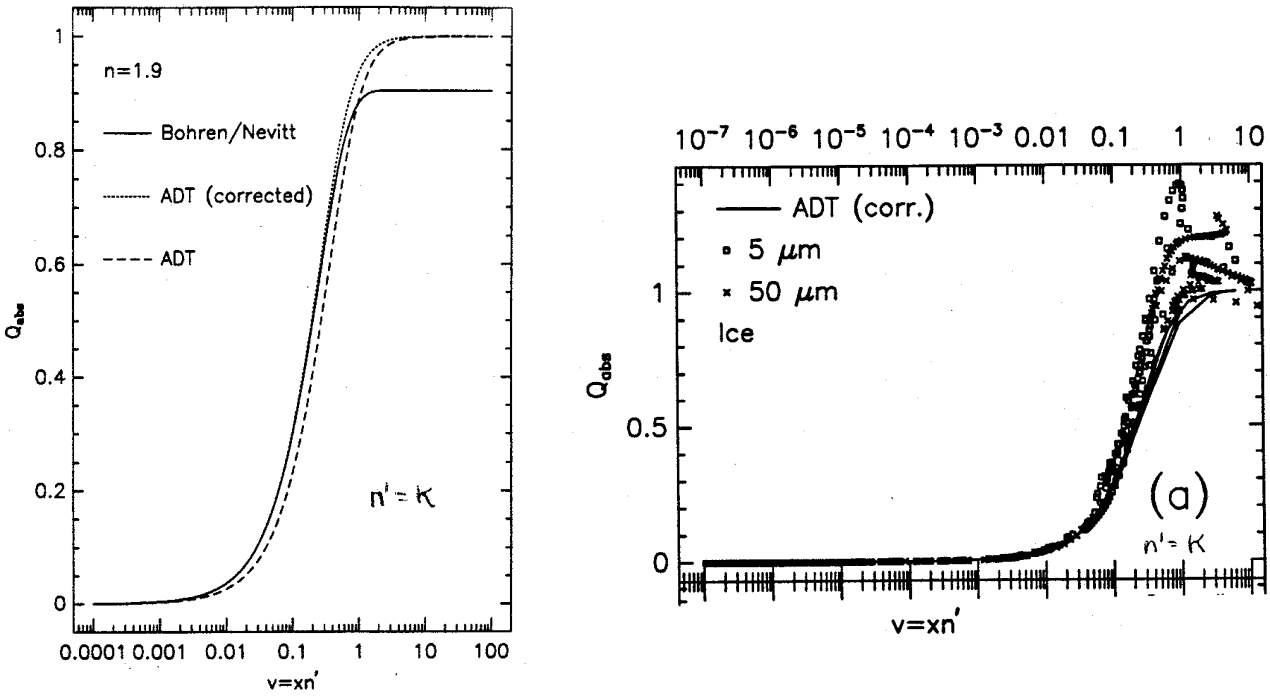


*Fig. 14.15 The absorption efficiency as a function of v. Spectra of $Q_{abs}$ and v as a function of wavelength for 5 μm and 10 μm water spheres.*

## 14.5 Extinction Coefficients and Optical Depths

The extinction coefficient (in this case, volume extinction coefficient) is defined as

$$\sigma_{ext} = \pi \int n(r) Q_{ext} r^2 dr \tag{14.21}$$

for spherical particles. Similar expressions apply to scattering and absorption. Based on dimensional arguments, $n(r) \rightarrow L^{-4}$, $r^2 \rightarrow L^2$, and $dr \rightarrow L$ and $\sigma \rightarrow L^{-1}$. *By* definition, the optical **depth** is

$$d\tau = \sigma_{ext} dz$$

*(a) Rayleigh Scatter (Liou, p76-79)*

$$\tau_{RAY}(p) = \int_p^0 \sigma_{ext}(p) \frac{dz}{dp'} dp'$$

$O_2$ and $N_2$ are conservative scatterers and the scattering cross section per unit molecule is

$$\sigma_{sca} = \frac{8\pi^3 (m^2 - 1)^2}{3\lambda^4 N_s^2} f(\delta),$$

where $f(\delta)$ accounts for depolarization effects induced by the nonsphericity of the molecule [$f(\delta) = (6 + 3\delta)/(6 - 7\delta)$], $\delta = 0.035$. The optical depth is thus

$$\tau(\lambda) = \sigma_{sca} \int N(z')dz'$$

where $N(z)$ is the number concentration of molecules as a function of height. Since this is proportional to pressure,

$$\tau(p, \lambda) = \tau_o(\lambda) p / p_o$$

A convenient parameterization of the Rayleigh optical depth is

$$\tau_{RAY}(z) = 0.0088\lambda^{-4.15+0.2\lambda} \exp[-0.1188z - 0.0016z^2]$$

where $z$ is expressed in km. The variation different than $\lambda^{-4}$ arises through the slight dependence of a (polarizability) on $\lambda$.

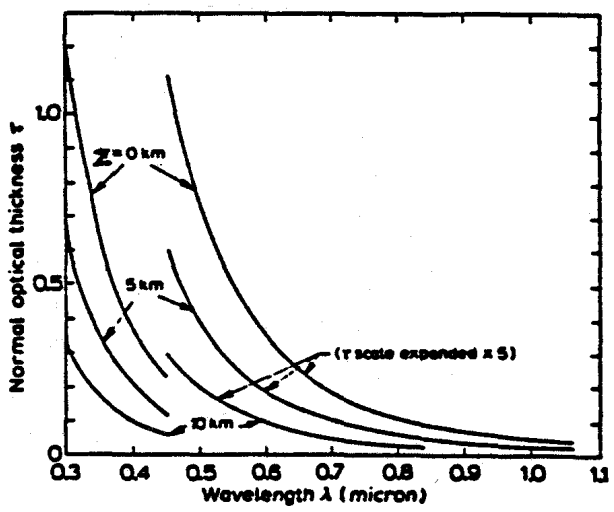


*Fig. 14.16 Rayleigh normal optical thickness between the top of the atmosphere and the altitudes given on the figure. (From Marggraf and Griggs, 1969).*

*(b) Cloud Optical Depth (at Solar Wavelengths)*

$$\tau_{cloud} = \int \sigma_{ext} dz$$

where

$$\sigma_{ext} = \int n(r) Q_{ext} \pi r^2 dr$$

At these wavelengths and for tropical cloud droplet sizes, $x >> 1$ so that

$$Q_{ext} \to 2$$

(the extinction paradox). Thus

$$\tau_{cloud} \cong 2 \iint n(r) \pi r^2 dr dz$$

With the following definitions

$$w = \frac{4}{3} \pi \rho \int n(r) \pi r^3 dr \qquad \text{(liquid water content)}$$

$$r_e = \int n(r) \pi r^3 dr \Big/ \int n(r) \pi r^2 dr \qquad \text{(effective radius)}$$

it follows that

$$\tau \sim \frac{3}{2} \frac{W}{r_e} \tag{14.22}$$

where $W = \int w(z') dz'$ = liquid water path. Thus extinction is inversely proportional to $r_e$ –this is important as it says that clouds composed of high concentrations of small droplets are optically thicker than clouds composed of fewer but larger droplets.

*(c) Cloud Optical Depth (IR)*

Let's suppose that only the absorption of IR radiation by cloud particle is important. Then the optical thickness is

$$\tau \sim \tau_{abs} \sim \int_0^{\Delta z} \int_0^{\infty} n(r) \pi r^2 Q_{abs} dr dz \tag{14.23a}$$

0 0

For IR wavelengths and cloud droplets ~ few microns, the size parameter is small and $Q_{abs}$ is approximately a linear function of $x$ and thus $r$ (e.g., Fig. 14.17).

To some limit, we can approximate $Q_{abs}$ by

$$Q_{abs} \sim \text{constant} \cdot r, \quad r < r_m$$

where $r_m$ is the characteristic radius of the distribution $n(r)$. On substitution

$$\tau_{abs} \sim \int_0^{\Delta z} \quad \text{constant} \quad \left\{ \int n(r) \pi r^3 dr \right\} dz$$

the terms in brackets is proportional to the cloud liquid water, therefore

$$\tau_{abs} \cong \text{constant} \cdot W \tag{14.23b}$$

where $W$ is cloud liquid water path.

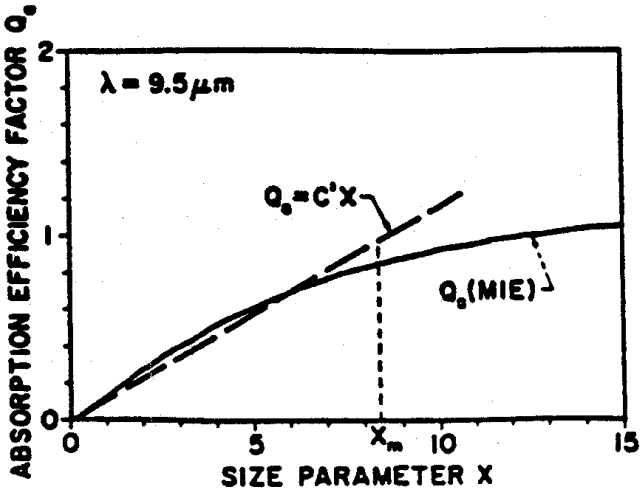


*Fig. 14.17 The Mie absorption efficiency $Q_s$ as a function of size parameter $x = (2\pi r/\lambda)$ and thus, of particle size for $\lambda = 9.5$ μm, $x_m$ corresponds to $2\pi r_m/\lambda$ where $r_m$ is referred to in the text (from Pinnick et al., 1979).*

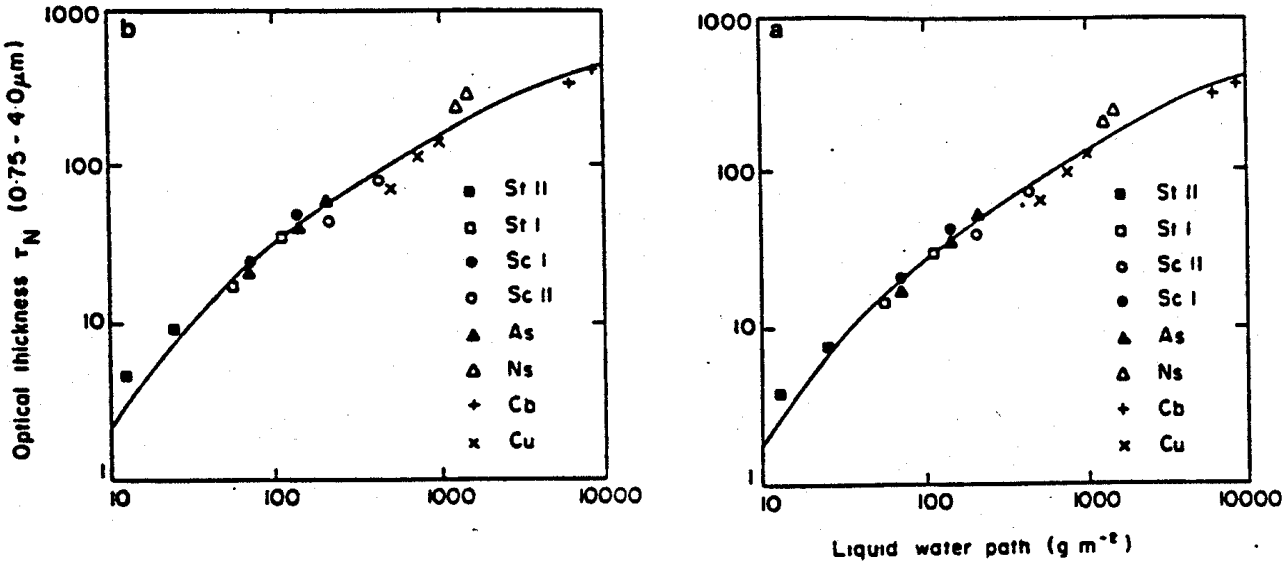


*Fig. 14.18 The broadband optical thickness for the 0.3—0.75 μm (a) and 0.75—4.0 μm (b) regions as a function of liquid water path and for several cloud types.*

## 14.6 Scattering Phase Function

The scattering pattern is described in terms of the amplitude function $S(\theta)$. We can gain a better grasp of this function by considering the following experiment. In this experiment, a particle of arbitrary shape is illuminated by a plane wave traveling from the negative $z$ direction as shown in Fig. 14.11. A detector is placed at $O'$ some distance $R$ from the particle and is moved around the particle at this distance. The field incident on the particle is

$$\mathcal{E}_{inc} = \mathcal{E}_o e^{-ikz+iwt}. \tag{14.24}$$

and the field measured at $O'$ is (refer to Eqn. (14.7))

$$\mathcal{E}_{sca} = S(\theta)\frac{e^{-ikR+iwt}}{kR}. \tag{14.25}$$

This field can be expressed in terms of the incident field at the particle by combining Eqns. (14.24) and (14.25)

$$\mathcal{E}_{sca} = S(\theta)\frac{e^{-ikr+ikz}}{kr}\mathcal{E}_o,$$

and in terms of intensities it follows that

$$I_{sca} = \frac{|S(\theta)|^2 I_o}{k^2 R^2}. \tag{14.26}$$

It is more usual to describe the angular patterns of scattered light in terms of a quantity referred to as the scattering phase function.[3] We can consider the relation of the phase function to the amplitude function in the following way. Consider an instrument located at the position at $O'$. If the area of the detector is $dA$, then the amount of radiation received by the detector is contained in the set of directions confined to a small solid angle element $d\Omega = dA/r^2$. Therefore the total energy per unit time at a given wavelength that is received by a detector capable of measuring the scattered radiation over the entire range of solid angles is

$$dw = I_{sca} dA \approx R^2 \int_{\Xi} I_{sca} d\Omega = \frac{I_o}{k^2}\int_{\Xi} |S(\theta)|^2 \, d\Omega \tag{14.27}$$

where $\Xi$ is used to denote the entire sphere of directions over which the integration is taken. Now we mentioned that the total amount of radiation scattered by a particle can be defined in terms of its scattering cross-sectional area $C_{sca}$. By definition,

$$I_o C_{sca} = R^2 \int_{\Xi} I_{sca} d\Omega, \tag{14.28}$$

[3] The use of the word phase to name this function has no relation to the phase of the wave but originates from the astronomical literature where it refers to lunar phases.

and

$$C_{sca} = \frac{1}{k^2}\int_{\Xi} |S(\theta)|^2 \, d\Omega \,. \tag{14.29}$$

These relationships provide us with the definition of the scattering phase function $P(\theta)$

$$\frac{P(\theta)}{r\pi} = \frac{|S(\theta)|^2}{k^2 C_{sca}} \tag{14.30}$$

which is a unitless quantity and when integrated over solid angle obeys the following condition

$$\frac{1}{4\pi}\int_{\Xi} P(\theta) d\Omega = 1. \tag{14.31}$$

This is an energy conservation condition, which simply states that in the absence of absorption the energy scattered in all directions around the particle must be just that amount that has been decreased from the original direction of propagation of the incident field.

Figure 14.19 presents plots of the phase function derived from Lorentz-Mie theory for spheres of varying size.

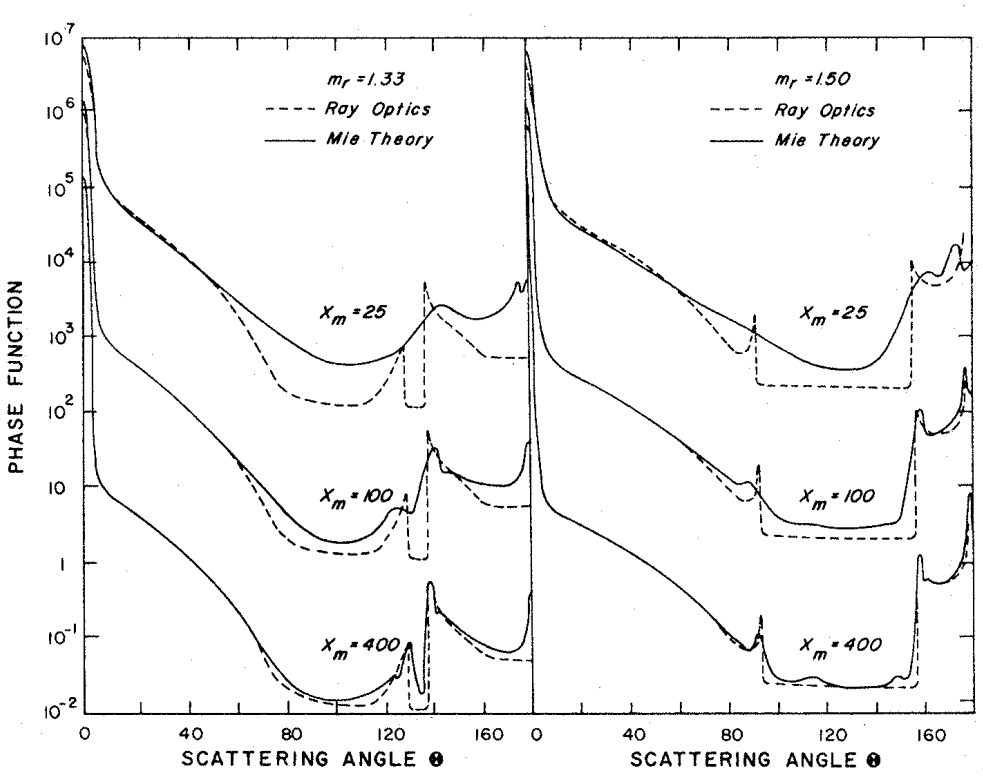


*Fig. 14.19 Comparison ray optics and Lorentz-Mie theory for phase functions derived from three size distributions ($x_m = 2\pi r_m/\lambda$) and two values of refractive index.*

*(a) Parameters of the Scattering Phase Function*

One parameter that usefully characterizes the asymmetry of particle scatter is the asymmetry parameter. It is defined as

$$g = \frac{1}{2}\int_{-1}^{+1} P(\cos\theta)\cos\theta d\cos\theta . \tag{14.32}$$

Note that $g = 1$ is complete forward scatter and $g = 0$ is isotropic and symmetric scatter (e.g., Rayleigh scatter).

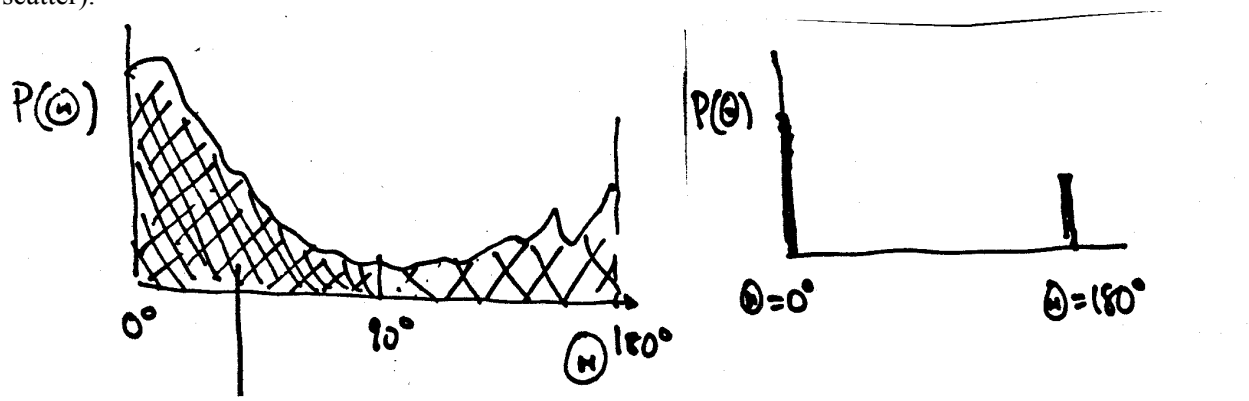


Consider as an example, the simplistic phase function shown below.

Forward scatter:

$$f = \frac{1}{4\pi}\int_0^{2\pi}\int_0^{1} P(\cos\theta)\sin\theta d\theta d\Phi$$

Backscatter:

$$b = \frac{1}{4\pi}\int_0^{2\pi}\int_{-1}^{0} P(\cos\theta)\sin\theta d\theta d\Phi$$

Normalization:

$$f + b = 1$$

For the simple phase function illustrated, it follows that

$$g = (+1)f + (-1)b$$

and

$$b = (1 - g)/2$$

$$f = (1 + g)/2$$

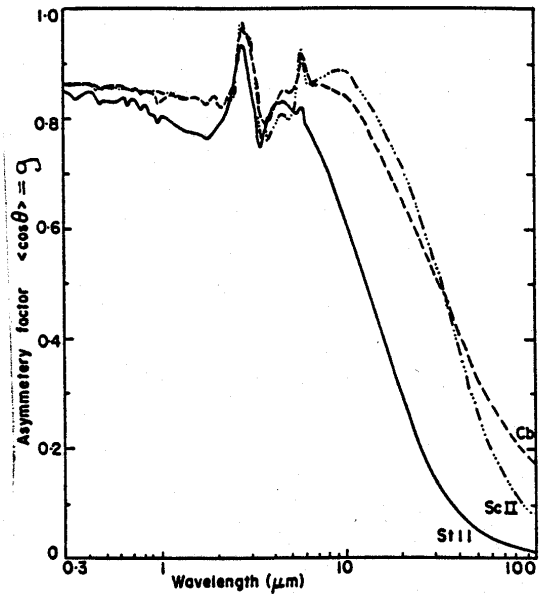


*Fig. 14.20 The asymmetry factor as a function of wavelength for the three cloud models.*

*(b) Simple Parameterization of the Scattering Phase Function*

We find it convenient to present the phase function by

$$P(\cos\theta) = \sum_{\ell=0}^{N} \chi_\ell P_\ell(\cos\theta)$$

where $P_\ell$ is the $\ell^{th}$ order Legendre polynomial and $\chi_\ell$ are the associated expansion coefficients. (Refer to exercise 14 (summer lecture course), for further discussion of phase function expansions.) A general rule of thumb is, the larger the particle the more terms are required to represent the phase function (Fig. 14.21).

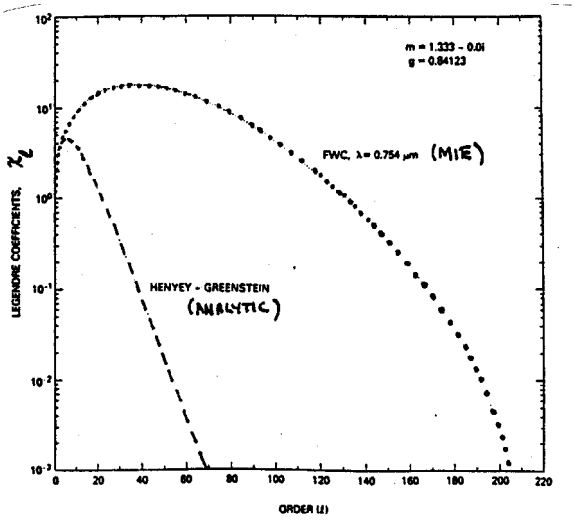


*Fig. 14.21 Coefficients of the Legendre polynomial expansion for a hypothetical cloud model derived for both Lorentz-Mie and Henyey-Greenstein phase functions.*

A specific form of phase functions useful in cloud calculations is the Henyey-Greenstein phase function. The H-C function decays monotonically with $\theta$ unlike real functions that possess glories, rainbows, and other optical phenomena (Fig. 14.22). It can be expressed in terms of $g$ as

$$P_{HG}(\cos\theta) = \frac{1 - g^2}{(1 + g^2 + 2g\cos\theta)^{3/2}}$$

which has a very convenient expansion

$$P_{HG}(\cos\theta) = \sum_{\ell} (2\ell + 1) g^{\ell} P_{\ell}(\cos\theta)$$

Combinations of H-G functions have been proposed to model the scattering in the back-hemisphere more realistically. An example is the double H-G function

$$\begin{aligned} P_{DHG} &= bP_{HG}(g_1) + (1-b)P_{HG}(g_2) \\ \overline{g} &= \text{effective asym. parameter} \\ &= bg_1 + (1-b)g_2 \end{aligned}$$

which is also graphically illustrated in Fig. 14.22c

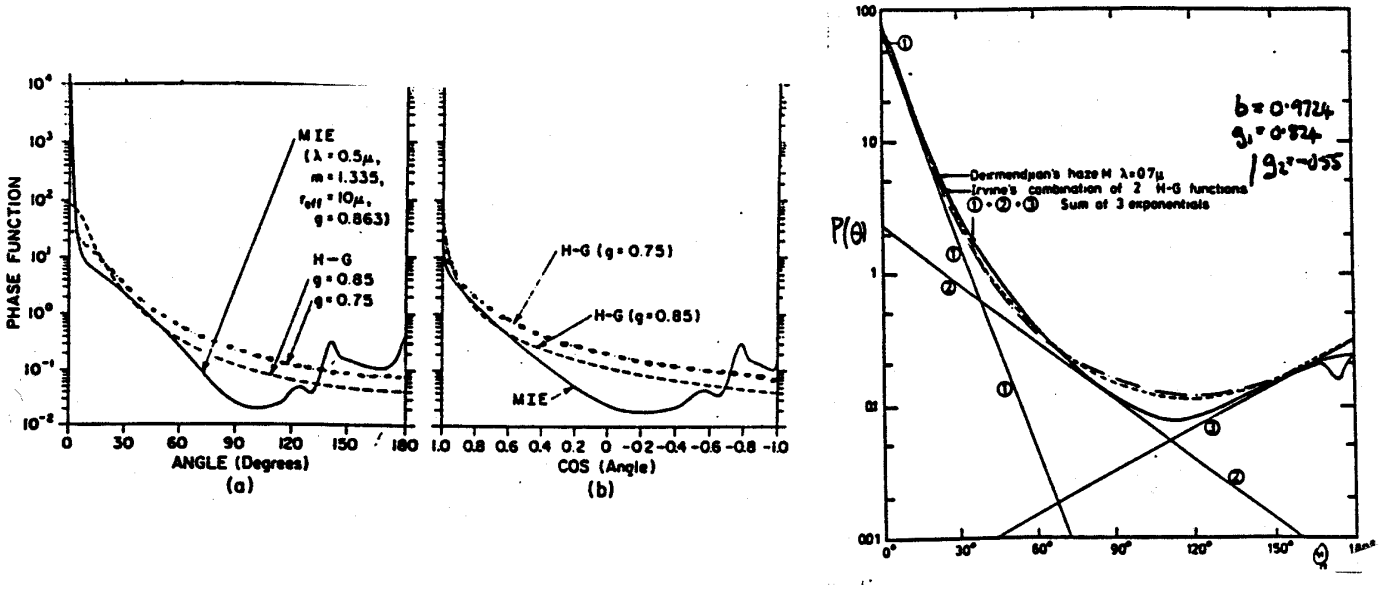


*Fig. 14.22 Comparison of three different phase functions plotted as functions of (a) $\theta$ and (b) cos $\theta$. Two are Henyey-Greenstein functions with g = 0.75 and 0.85 and with values at $\theta$ = 0 of 28 and 86, respectively. The third is a Lorentz-Mie case for a polydisperse water cloud of effective radius 10 μm, with a value of 9.7 x $10^3$ at $\theta$ = 0. (c) Example of a double H-G function with the values of b, $g_1$ and $g_2$ as indicated.*

## 14.7 Scattering by Spheres: A Brief Outline of Lorentz-Mie Theory

The theory for scattering by dielectric spheres was developed independently by Lorentz in 1890 and Gustav Mie in 1908 (refer to the discussion of these developments in the bibliographical discussions at

the end of this chapter). The derivation of the solution is a straightforward application of classical electromagnetic theory so only the resulting formulae are given here.

*(a) General Formulae*

Mie's solutions for scattering by a dielectric sphere are infinite series whose rates of convergence depend on the value of the size parameter $x$. The two scattering amplitude functions have the form

$$S_1(\theta) = \sum_{n=1}^{\infty} \frac{2n+1}{n(n+1)} [a_n \pi_n(\cos\theta) + b_n \tau_n(\cos\theta)], \tag{14.33a}$$

$$S_2(\theta) = \sum_{n=1}^{\infty} \frac{2n+1}{n(n+1)} [a_n \tau_n(\cos\theta) + b_n \pi_n(\cos\theta)], \tag{14.33b}$$

where

$$\begin{aligned} \pi_n(\cos\theta) &= \frac{1}{\sin\theta} P_n^1(\cos\theta) \\ \tau_n(\cos\theta) &= \frac{d}{d\theta} P_n^1(\cos\theta), \end{aligned} \tag{14.34}$$

and where $P_n^1$ is the associated Legendre polynomial (e.g., Abromowitz and Stegun 1971). The coefficients $a_n$ and $b_n$ are referred to as Mie scattering coefficients and are functions of refractive index $m$ and size parameter $x$. The mathematical forms of these coefficients are given as ratios of Ricatti-Bessel functions. The extinction and scattering efficiencies are also series

$$Q_{ext} = \frac{2}{x^2} \sum_{n=1}^{\infty} (2n+1) \operatorname{Re}(a_n + b_n) \tag{14.35a}$$

$$Q_{sca} = \frac{2}{x} \sum_{n=1}^{\infty} (2n+1)(|a_n|^2 + |b_n|^2). \tag{14.35b}$$